Cold Test 3, Run 3
Spartan IR Camera for the SOAR Telescope

Dustin I. Baker & Edwin D. Loh

Department of Physics & Astronomy
Michigan State University, East Lansing, MI 48824

`Loh@msu.edu`   517 355–9200 x2480

07 October 2007

Abstract

This note reports the results of Run 3 of Cold Test 3. During Run 2, we found that a light leak dominated the dark current. We fixed several suspected sources of light leaks and measured the dark current to be 1–$3\,e^-/s$, which is a factor of 3 lower than for Run 2. The dark current is about 1/10 of the sky flux for the high-res configuration in the J band, the darkest band.

The 4-eye detector mechanism did not move properly. The strings that drive the mechanism are teflon-coated quartz. When cold, the teflon becomes stiff and causes a string to become stuck where it bends.

One string became frayed.

The rotation stages for the big filter wheel and the mask wheel jammed for $0.2\,s$ when run for the first time after cool down.

1   Introduction

Run 3 of Cold Test 3 began on 30 May 2007 and ended abruptly on 20 June, when the instrument fell. For the results of Run 2 (22 January–10 March 2007), see Baker & Loh 2006[1]

1.1   Tests

Measure dark current Use the dark slide. Measure with detector 1, which glows, on and off.

Test 4-eye mechanism Measure the image position at several positions of the wide-field camera mirror, which drives the 4-eye mechanism. If the mechanism

---

[1]Baker, D., & Loh, E., 2006, Cold test 3, run 2, Spartan IR Camera for the SOAR telescope.

works properly, the image shifts as the mirror moves even when the mirror does not intercept the light beam.

1.2   Installation

The bottom of the instrument is the side with the conflat vacuum opening for filter access. The window is on the front side.

The detector locations are named A1, A2, B1, and B2, where the "B" detectors are closer to the exterior of the instrument and the "2" detectors are toward the top (Figure 1).
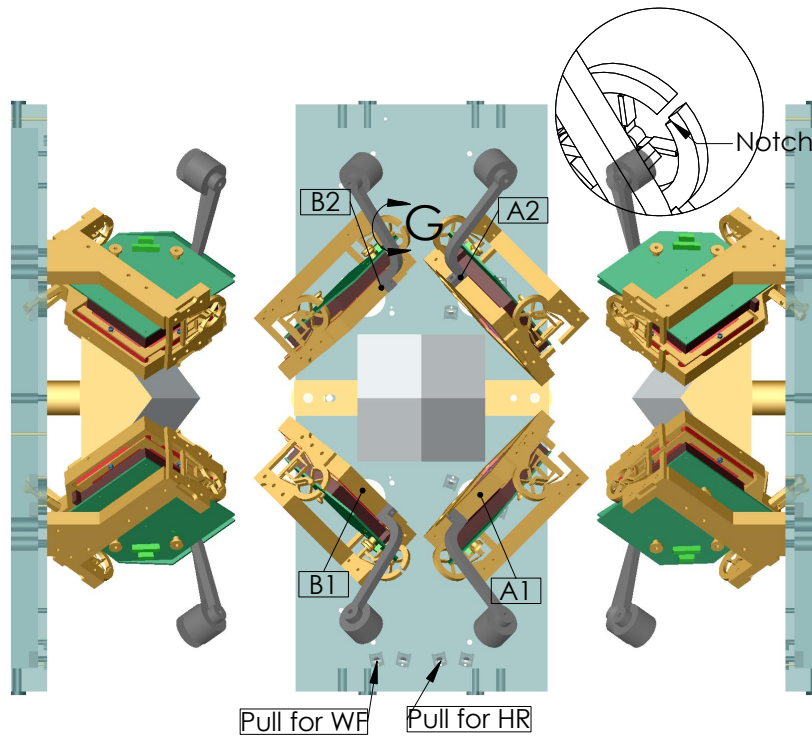

Figure 1: The 4-eye detector assembly shown in the wide-field configuration. Note the detector locations A1, A2, B1, and B2. The top of the instrument is at the top. The magnified detailed view shows the notch on the axles for the B detectors. The rotation axis, which points up before reflection by the pyramidal mirror, points NW, NE, NE, and NW for the A2, B2, A1, and B1 detectors, respectively, after reflection. The rotatation is right-handed for the wide-field configuration and left-handed for the high-res configuration.

The detectors are installed according to Table 2, and Table 1 shows their connections to the vacuum bulkheads and detector controllers. The channel numbers refer to the inputs on the umbilical board.

	Bottom					*Top*			
Pins	*Posn.*	*Contr.*	*Pins*	*Contr.*	*Pins*	*posn.*	*Contr.*	*Pins*	*Contr.*
20	A1	3			30	B2	7		
30	A1	3			20	B2	7		
20	nc		10	3	30	A2	2	10	nc
30	B1	5			20	A2	2		
20	B1	5			30	nc			
30	nc				20	nc			

Table 1: Vacuum bulkhead for the detector cables. The bulkhead is oriented as viewed from the air side; the 10-pin cable is to the right of the 20 and 30-pin cables.

Chan.	*Cont. SN*	*Loc.*	*Det. SN*	*Grade*
0	3	A1	24	Science
1	5	B1	92	Engineering
2	2	B2	97	Engineering
3	7	A2	66	Science

Table 2: Detectors. The channel number determines rotation of the FITS file.

Pinholes on a mask plate are used to make artificial stars (Figure 3). There are three requirements. (1) Focus all four detectors over a range of $(-1,+1)$ mm in order to see a substantial change in the image. Use wells that are 0.9 and 1.5 mm deeper to cover the negative range. Put pinholes on washers to cover the positive range. (2) Measure the tilt for all four detectors. For that, pinholes need to cover the full range of distances from the rotation axis of 4-eye. The projection of the rotation axis onto the mask is the vertical axis in Figure 3. Pinholes at A5–A8 and B5–B8 are used to measure the tilt for two detectors. They need to be rotated slightly to measure tilt for the other two detectors. (3) Cover the corners and center of the field to evaluate the image over the field.
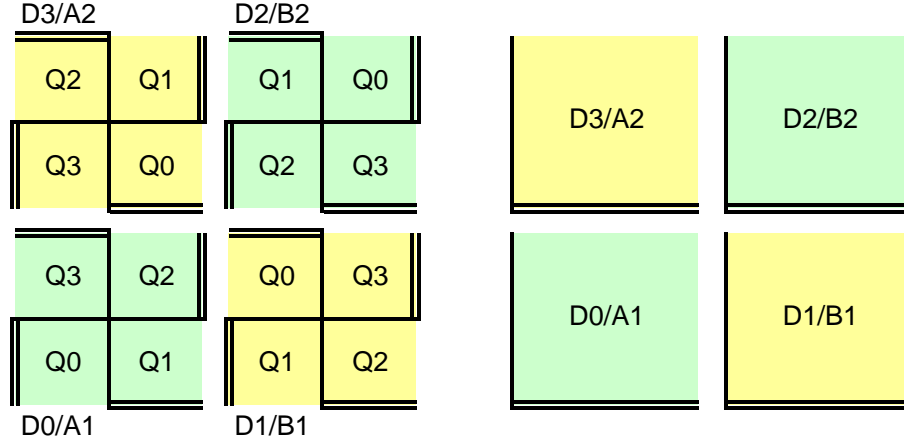
3

Figure 2: Detector arrangement. The x-axis, which changes more rapidly in the image file, is shown with double lines, and the single line is the y-axis. The right panels show the entire detector, and the left panels show the separate quadrants.
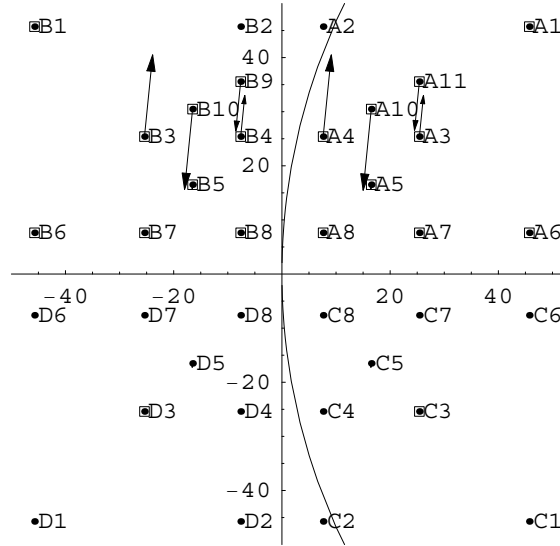

Figure 3: Pinholes (squares) for run 3 of cold test 3, as viewed from the front of the instrument with the top up. The unused wells are shown as points. The arrows indicate the axial offset from the curved focal surface of the telescope, where up in the figure is toward the interior of the instrument. The curved line is the position of the center of the mask as the mask wheel rotates. If the mask is centered, the A, B, C, and D pinholes image onto the detectors at B1, A1, B2, and A2, respectively.

Loc.	Offset [mm]	
A3	0.76	on washer
A4	0.91	on washer
A10	−1.5	deep well
A11	−0.9	deep well
B3	1.51	on washer
B4	0.55	on washer
B9	−0.91	deep well
B10	−1.48	deep well

Table 3: Pinholes that are offset from the focal surface of the telescope

2   Detector Mechanism

To determine whether the 4-eye mechanism actually tilts the detectors, we moved the wide-field camera mirror in 5° and 10° steps from $\alpha = 0°$, its wide-field position, to 90°, where it, being out of the beam, lets the light hit the high-res camera mirror. The mechanism for the wide-field camera mirror drives the 4-eye mechanism. At $\alpha < 45°$, the mechanism pulls strings to tilt 4-eye toward the wide-field position, and at $\alpha > 45°$ it pulls another set of strings to tilt 4-eye toward the high-res position. There are stops at $\alpha = 0°$ and 90°.
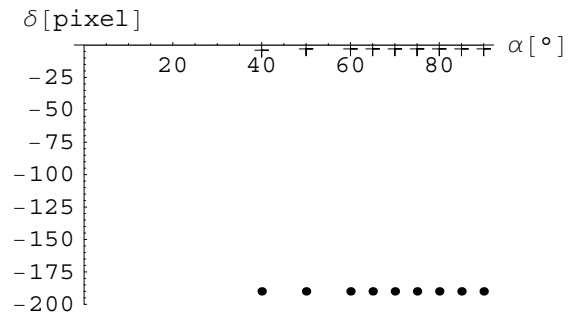

Figure 4: Shift of the position of the secondary image formed by the high-res camera mirror for quadrant 3 of detector 0 in the symmetric (plus) and asymmetrc (point) directions vs. angle α of the low-res camera mirror. The mirror is in the low-res position at $\alpha = 0°$. The secondary image is not visible at smaller angles, because the low-res camera mirror blocks the high-res camera mirror.

The 4-eye mechanism does not work properly at the high-res position. The image should move as the wide-field camera mirror moves near $\alpha = 90°$, but it does not (Figure 4).

The image moves as the wide-field camera mirror moves near $\alpha = 0°$ (Figure 5). The image moves for two reasons. First, wide-field camera mirror turns about a rotation axis that is 1.4 mm from the mirror axis, and the normal of the mirror surface for a given light bundle changes slightly. (If the rotation axis were coincident with the mirror axis, the image would not move.) This causes motion in both the direction of symmetry of the instrument and the asymmetric direction. The second reason is that the detector tilts between the wide-field and high-res modes. The tilt moves the image only in the asymmetric direction, since its rotation axis is parallel to the direction of symmetry.

The 4-eye mechanism works properly at the wide-field position. The rotation of the mirror cannot account completely for the movement of the image in the asymmetric direction (top-right panel of Figure 5). Removing the effect of the mirror position (lower panels of Figure 5) reveals the tilt of the detector. Near $\alpha = 45°$, the strings are slack, and the detector tilt does not change. As α nears 0°, the strings tighten and pull against the spring of the Henein axles.

The detector mechanism hits the stops in the wide-field mode for detectors 0, 2, and 3. The fit of the image movement for $10° \leq \alpha \leq 30°$ hits zero around $\alpha = 5°$

(lower panels of Figure 5). This is also the case for detector 2, although it is not shown. We have no measurement for detector 1, since no pinholes imaged onto it for our pictures.
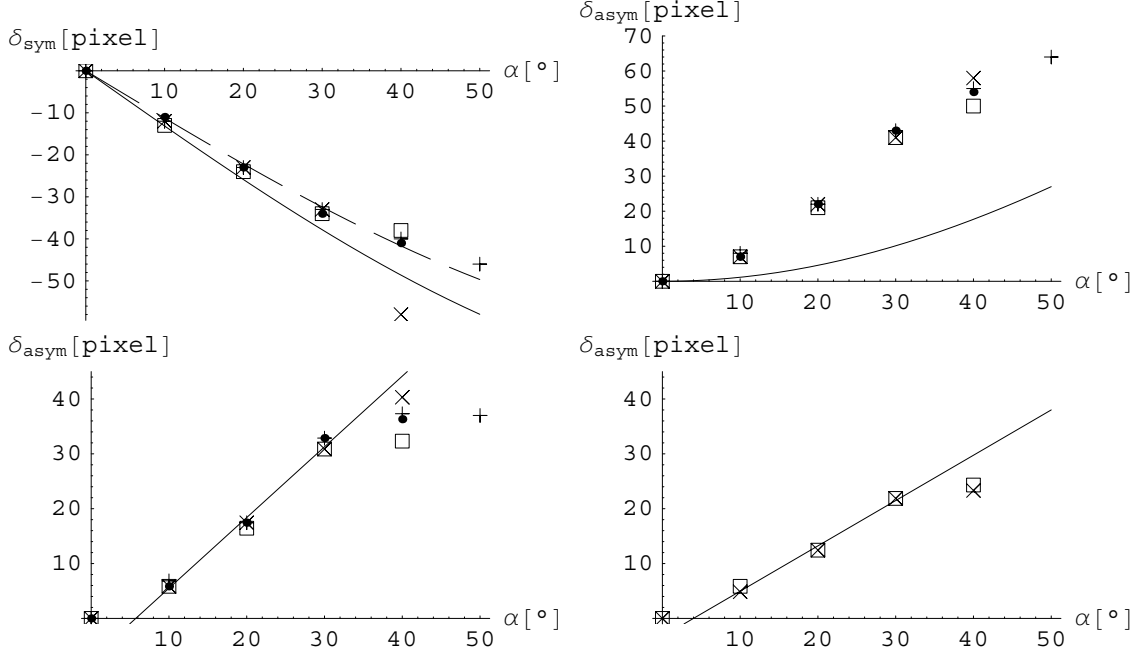

Figure 5: Shift of the image position for detector 0 in the symmetric (top left) and asymmetric (top right) directions vs. angle α of the low-res camera mirror. The solid line is the computed shift due to the change in the mirror position alone and not accounting for the tilt of the detector. The dashed line is the shift computed with the rotation axis moved from 1.4 mm from the optic axis, the nominal distance, to 1.2 mm. The mirror is in the low-res position at $\alpha = 0$. The image is not visible at greater angles. In the lower panels (detector 0 on the left and detector 3 on the right), the effect of the mirror position has been removed to show the movement due to the tilt of the detector. The symbols are point, plus, cross, and square for quadrants 0, 1, 2, and 3, respectively.

2.1 Stiff strings

The strings by which the mechanism for the wide-field camera mirror tilt the detectors make three bends of at least 90°, and we believe that the strings become stiff at cold temperatures and cannot move around the bends.

From the driving mechanism to the detector, the strings (1) make a 90-degree bend around a ϕ4.7-mm roller bearing, (2) connect to a spring that compensates for the differential contraction between the quartz string and the cryo-optical box, (3) make another 90-degree bend around a ϕ4.7-mm roller bearing, and (4) make a bend around a surface with a varying radius of curvature. The strings accomodate the first bend, since they are connected directly to the driving mechanism. However, the spring limits the tension at the second and third bends.

We measured the tension needed to move the strings at the second and third bends. For the measurement at 77 K, we submerged the 4-eye assembly in liquid nitrogen. With the strings doubled at the second bend and quadrupled at the third bend, the tension to move a single eye is 1.3 N at room temperature and 5.0 N at 77 K. With the strings doubled at both bends, the tension to move a single eye is 0.6 N at room temperature and 2.9 N at 77 K.

Because the frictional force should be independent of the number of strings at room temperature, we suspect that in the case of quadrupled strings a string may have overlaid another to increase the friction.[2]

The tension on the spring is 6 N, whereas it takes 12 N to move four eyes with doubled strings.

Several improvements are possible: (1) Use a stiffer spring to increase the tension. (2) Rather than quadrupled or doubled strings, use single strings to prevent one string from overlaying another. (3) Move the spring from between the first and second bends to a point between the second and third bends, which requires 4 or 8 springs instead of 2, the current number.

2.2   Inspection of the 4-eye mechanism

One string is frayed at the roller bearing nearest the wide-field camera mirror.

---

[2]When a string overlays another, the friction between the top string and the smooth surface is replaced by an equal increase in friction between the bottom string and the surface and an additional friction between the two strings. The friction between two strings is large because the strings are made of many strands, like a rope.

3   Dark Current

In Run 2, the dark current depended on the ambient temperature, which means it was caused by thermal radiation from the instrument walls leaking onto the detector.[3] We suspect that the path of the leak is from the instrument walls through unclosed joints in the insulating blankets through holes in the cryo-optical box (COB).

For this run, we attempted to fix the light leak. We stitched the pieces of the insulating blankets together. We plugged with bolts a score of ϕ6-mm bolt holes, a score of ϕ3-mm bolt holes, and six ϕ6-mm holes for reference pins in the COB. We put pieces of black aluminum foil on 4 ϕ6-mm holes for reference pins for the 4-eye assembly. We hid a ϕ19-mm hole for temperature sensors with black aluminum foil. The most important light leak is probably through this hole, since the detectors see this hole. We left uncovered five ϕ19-mm holes for

Figure 6: Light vs integration time for quadrant q on detector d. Detector 1 is on for the top panel and off for the bottom panel.

motor wires, because they are not likely to be a problem and they are difficult to cover. For four of these in the bright chamber of the COB, light would have to go through the Lyot stop and make several reflections to get to the detector. One in the dark chamber is hidden behind a wall.

The dark current was measured by inserting a dark slide in place of the Lyot stop and inserting the mask at the telescope focus. Since there are openings in the mask where there are no pin holes, there is some light in the bright chamber of the COB. The results are in Figure 6.

The dark current is higher when detector 1 is turned on. Detector 1, serial number 92, emits light.[4] The dark current is higher by a factor 1.8, 2.8, and 1.6 for detectors 0, 2, and 3, respectively. (See Table 4.) The dark current due to detector 1 is 0.2,
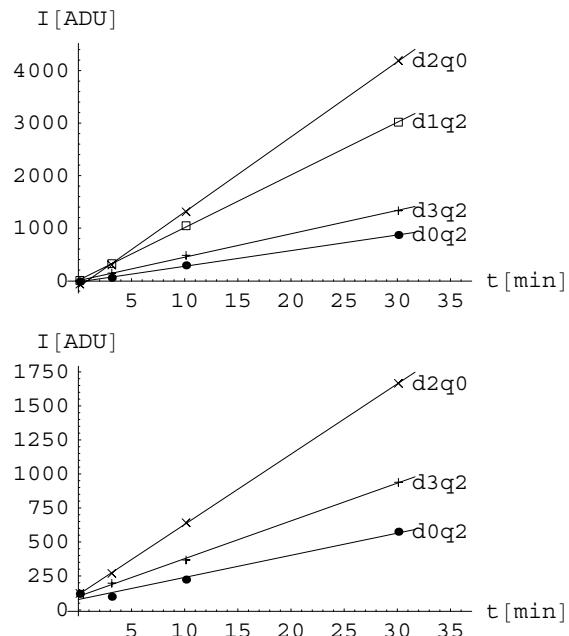
---

[3]Baker, D., & Loh, E., 2007, Cold test 3, run 2, Spartan IR Camera for the SOAR telescope, §5
[4]Baker, D., & Loh, E., 2007, *Ibid.*, §5.2.

1.5, and $0.3\,\mathrm{ADU/s}$ for detectors 0, 2, and 3, respectively.

Stopping the light leaks lowered the dark current by a factor of 3–4 (last column in Table 4).

The conversion from ADU to electrons is 3.08 ± 0.05, 3.02 ± 0.07, and $(2.44 \pm 0.01)\,\mathrm{e^-/ADU}$ for detectors 0, 1, and 3.[5] The conversion for detector 2 is assumed to be $3.0\,\mathrm{e^-/ADU}$.

det.	SN	$I_{1\mathrm{off}}$ [ADU/s]	$I_{1\mathrm{off}}$ [e$^-$/s]	$I_{1\mathrm{on}}$ [ADU/s]	$I_{1\mathrm{on,r2}}$ [ADU/s]	$I_{1\mathrm{off,r2}}$ [ADU/s]	$I_{1\mathrm{off,r2}}/I_{1\mathrm{off}}$
0	24	0.3	0.8	0.5		0.9	3.3
1	92			1.7	3.1		
2	97	0.9	2.6	2.4			
2	74					4.2	
3	66	0.5	1.1	0.7		1.9	4.0

Table 4: Dark current with detector 1 turned off, $I_{1\mathrm{off}}$, with detector 1 turned on, $I_{1\mathrm{on}}$, and that during run 2 of cold test 3, $I_{1\mathrm{off,r2}}$ and $I_{1\mathrm{off,r2}}$. The values of $I_{1\mathrm{off,r2}}$ and $I_{1\mathrm{off,r2}}$ have been converted to the current gain of the electronics.

The measured dark current is a factor of 3 (for detector 0) to 10 (for detector 2) higher than the specification. The specification for the dark current is $0.03\,\mathrm{e^-/s}$ at 78 K. Ideally, the dark current changes with temperature as $\exp(-E/(kT))$, where E is half the energy of the band gap. The cut-off wavelength is 2500 nm. Therefore the expected dark current is $0.3\,\mathrm{e^-/s}$ at 83 K, the temperature on the sensor on the circuit board behind the detector. It is possible that light leaks remain.

At the telescope, we estimate the dark current to be lower by a factor of 3, if the dark current is not due to a light leak. The pressure on Cerro Pachon, which is 2.7 km above sea level, is 0.72 that at sea level according to the Standard Atmosphere. Using the Clausius-Claperyon equation, we expect the boiling point of nitrogen to be lower by 2.8 C.

If the dark current is caused by a light leak, we estimate the dark current to be lower by a factor of 2.3 at the telescope where the ambient temperature is expected to be 10 C, rather than 22 C in the laboratory.

---

[5]*Ibid.*, p. 32.

3.1 Dark current and observing

The dark current is much lower than the flux from the sky in the J band in the high-res configuration, which has the darkest sky (column 4 of Table 5). The estimated sky flux is $17\,\mathrm{e^-/s}$ for those conditions[6]

The dark current will be brighter than the sky flux in a HeI ($\lambda 1083\,\mathrm{nm}$) filter. Since the 10-nm wide HeI filter[7] is narrower than the 280-nm wide Mauna Kea J filter,[8] the sky will be darker by a factor of a 28.

det.	*SN*	$I_{1\mathrm{off}}$ $[\mathrm{e^-/s}]$	$I_{1\mathrm{off}}/B_{\mathrm{J}}$	$I_{1\mathrm{off}}/B_{\mathrm{HeI}}$
0	24	0.8	0.05	1.4
1	92	5.	0.3	8.
2	97	2.6	0.15	4.
3	66	1.1	0.07	2.

Table 5: Dark current summary. For the measurements with detector 1, detector 1 is turned on, of course.

4 Rotation stages

During run 2, the rotation stage for the mask wheel jammed when it was moved for the first few times after cooling down.[9] We replaced its motor driver, NI 7604, which supplies up to $1.0\,\mathrm{A}$ RMS, with Prismatics MDM2200, which supplies more than the 2.0-A RMS current that saturates the magnets.

Increasing the motor current did not fix the problem. For this run, the rotation stages for the big filter wheel and the mask wheel jammed when run for the first time after cool down. The duration of jamming was brief, because the reverse limits moved only by about $0.5°$, which translates to a time of $0.2\,\mathrm{s}$.

---

[6]Loh, E., 2007, Observing Manual, Spartan IR Camera.

[7]Downey, E., 2006, Barr Associates, quote for Cassio Barbosa of UNIVAP.

[8]Simons, D. A., & Tokunaga, A., 2002, The Mauna Kea Observatories Near-Infrared Filter Set. I. Defining Optimal 1–5 Micron Bandpasses, PASP, 114, 169.

[9]Baker, D., & Loh, E., 2007, Cold Test 3, Run 2, Spartan IR Camera for the SOAR Telescope, p. 7.